雑誌

発表者氏名	論文タイトル名	発表誌名	巻号	ページ	出版年
Lee JA, Madrid RE, Sperle K, Ritterson CM, Hobson GM, Garbern J, Lupski JR, Inoue K.	Spastic paraplegia type 2 associated with axonal neuropathy and apparent *PLP1* position effect.	*Ann Neurol*	59(2)	398-403.	2006
Lee JA, Inoue K, Cheung SW, Shaw CA, Stankiewicz P, Lupski JR.	Role of genomic architecture in *PLP1* duplication causing Pelizaeus-Merzbacher disease.	*Hum Mol Genet*	15(14)	2250-2265	2006
Kim, B. Y., Sahara, Y., Yamamoto, A., Kominami, E., Kohsaka, S., and Akazawa, C.	The interaction of mammalian Class C Vps with nSec-1/Munc18-a and syntaxin 1A regulates presynaptic release.	*Biochem. Biophys. Res. Comm.*	350	691-697	2006
Yogosawa, S., Kawasaki, M., Wakatsuki, S., Kominami, E., Shiba, Y., Nakayama, K., Kohsaka, S. and Akazawa, C.	Monoubiquitylation of GGA3 by hVPS18 regulates its ubiquitin-binding ability.	*Biochem. Biophys. Res. Comm.*	350	82-90	2006

Akazawa, C., Nakamura, Y., Maeno, H., Wada, K. and Kohsaka, S.	Distribution of the Serum inducible kinase (Snk) mRNA in the rat nervous system; its up-regulation in lateral and basolateral amygdala after cued fear conditioning.	Submitted			
Koizume, S., Takizawa, S., Fujita, K., Aida, N., Yamashita, S., Miyagi, Y., and Osaka, H	Aberrant trafficking of a proteolipid protein in a mild Pelizaeus-Merzbacher disease.	*Neuroscience*	141	1861-1869.	2006
Sato, A., Arimura, Y., Manago, Y., Nishikawa, K., Aoki, K., Wada, E., Suzuki, Y., Osaka, H., Setsuie, R., Sakurai, M., *et al.*	arkin potentiates ATP-induced currents due to activation of P2X receptors in PC12 cells.	*J Cell Physiol.*	209	172-182	2006
Setsuie, R., Wang, Y. L., Mochizuki, H., Osaka, H., Hayakawa, H., Ichihara, N., Li, H., Furuta, A., Sano, Y., Sun, Y. J., *et al.*	Dopaminergic neuronal loss in transgenic mice expressing the Parkinson's disease-associated UCH-L1 I93M mutant.	*Neurochem Int.*	50(1)	119-129	2007

Sun, Y. J., Nishikawa, K., Yuda, H., Wang, Y. L., Osaka, H., Fukazawa, N., Naito, A., Kudo, Y., Wada, K., and Aoki, S. (2006).	Solo/Trio8, a membrane-associated short isoform of Trio, modulates endosome dynamics and neurite elongation.	*Mol Cell Biol*	26	6923-6935	2006
Wang, Y. L., Liu, W., Sun, Y. J., Kwon, J., Setsuie, R., Osaka, H., Noda, M., Aoki, S., Yoshikawa, Y., and Wada, K.	Overexpression of ubiquitin carboxyl-terminal hydrolase L1 arrests spermatogenesis in transgenic mice.	*Mol Reprod Dev*	73	40-49	2006
Takahashi, Y, Matsuda, K, Kubota Y, Shimomura J, Yamasaki, E, Kudo, T, Fukushima K, Osaka H, Akasaka N, Imamaura , A, Yamada, S, Kondo, N, Fujiwara, T	Vaccination and infection as causative factors in Japanese patients with Rasmussen syndrome: Molecular mimicry and HLA class I	*Clin Dev Immunol.*	13	381–387	2006
Koizume S, Nagai J-i, Miyagi Y and Osaka H.	Varied missense mutations or expression condition modulates trafficking and quality control of proteolipid proteins	In preparation			

Deguchi K, Takashima S, Armstrong DL, Inoue K.	Brains of extremely premature infants with white matter injury also exhibit altered neural progenitor cells and cortical development.	In preparation			

研究成果の刊行物・別刷（抜粋）

Human Molecular Genetics, 2006, Vol. 15, No. 14 **2250–2265**
doi:10.1093/hmg/ddl150
Advance Access published on June 14, 2006

Role of genomic architecture in *PLP1* duplication causing Pelizaeus-Merzbacher disease

Jennifer A. Lee[1], Ken Inoue[3], Sau W. Cheung[1], Chad A. Shaw[1], Pawel Stankiewicz[1] and James R. Lupski[1,2,4,*]

[1]Department of Molecular and Human Genetics, [2]Department of Pediatrics, Baylor College of Medicine, One Baylor Plaza, Room 604B, Houston, TX 77030, USA, [3]Department of Mental Retardation and Birth Defect Research, National Institute of Neuroscience, National Center of Neurology and Psychiatry, Kodaira, Tokyo 187-8502, Japan and [4]Texas Children's Hospital, Houston, TX 77030, USA

Received April 18, 2006; Revised and Accepted June 6, 2006

Genomic architecture, higher order structural features of the human genome, can provide molecular substrates for recurrent sub-microscopic chromosomal rearrangements, or may result in genomic instability by forming structures susceptible to DNA double-strand breaks. Pelizaeus-Merzbacher disease (PMD) is a genomic disorder most commonly arising from genomic duplications of the dosage-sensitive proteolipid protein gene (*PLP1*). Unlike many other genomic disorders that result from non-allelic homologous recombination utilizing flanking low-copy repeats (LCRs) as substrates, generating a common and recurrent rearrangement, the breakpoints of *PLP1* duplications have been reported not to cluster, yielding duplicated genomic segments of varying lengths. This suggests a distinct molecular mechanism underlying *PLP1* duplication events. To determine whether structural features of the genome also facilitate *PLP1* duplication events, we analyzed extensively the genomic architecture of the *PLP1* region and defined several novel LCRs (LCR–PMDs). Array comparative genomic hybridization showed that *PLP1* duplication sizes differed, but revealed a subgroup of patients with apparently similar *PLP1* duplication breakpoints. Pulsed-field gel electrophoresis analysis using probes adjacent to the LCR–PMDs detected unique recombination-specific junction fragments in 12 patients, enabled us to associate the LCR–PMDs with breakpoint regions, and revealed rearrangements inconsistent with simple tandem duplications in four patients. Two-color fluorescence *in situ* hybridization was consistent with directly oriented duplications. Our study provides evidence that *PLP1* duplication events may be stimulated by LCRs, possibly non-homologous pairs at both the proximal and distal breakpoints in some cases, and further supports an alternative role of genomic architecture in rearrangements responsible for genomic disorders.

INTRODUCTION

Architectural features of the human genome can result in genome instability, and susceptibility to rearrangements resulting in disease traits. Such rearrangements, including deletions, duplications and inversions at specific regions may result in the loss or gain of a dosage-sensitive gene (or genes), disruption of a gene, generation of a novel gene at the breakpoints, or dysregulation of a gene in proximity to the rearrangement, causing what is termed a genomic disorder (1–3). Genomic disorders represent a wide spectrum of unrelated clinical conditions including, for example, Charcot-Marie-Tooth disease type 1A (4,5), Smith-Magenis syndrome (6,7) and Williams syndrome (8,9). Yet, the underlying molecular basis is the same: rearrangement involving specific genomic segments ranging from a few kilobases (kb) to several megabases (Mb) in length (10). Many genomic disorders share a common mechanism for their underlying rearrangement: non-allelic homologous recombination (NAHR) between low-copy repeats (LCRs) that flank the rearranged genomic segment (1). Such rearrangements yield common recombinant genomic segments. However, some

*To whom correspondence should be addressed. Tel: +1 7137983723; Fax: +1 7137985073; Email: jlupski@bcm.tmc.edu

genomic disorders, and selected rearrangements for specific genomic disorders, that deviate from this classic model exist.

Among them is Pelizaeus-Merzbacher disease (PMD), a rare X-linked dysmyelinating disorder of the central nervous system (CNS) (11–13). PMD most commonly (60–70%) arises from genomic duplications of the dosage-sensitive proteolipid protein gene (*PLP1*) (14,15) located on chromosome Xq22.2 (16,17), and less commonly by *PLP1* deletions (18) and point mutations (11). Both the deletions (18) and duplications (19) causing PMD appear to arise by non-homologous end joining (NHEJ) as surmised from the nucleotide sequence of the products of recombination. However, what makes the genomic region surrounding *PLP1* susceptible to rearrangement remains to be elucidated. PLP1 is an integral membrane protein and the most abundant component of myelin in the CNS; an extra copy of *PLP1* resulting from whole gene duplication affects the development of oligodendrocytes. Specifically, PMD caused by *PLP1* duplication is characterized by oligodendrocyte cell death and abnormal CNS myelination (20).

Many genomic disorders result from homologous recombination between non-allelic LCRs, yielding recombination products with common breakpoints. Interestingly, in PMD patients with *PLP1* duplication, the rearrangement breakpoints are not common, yielding duplicated genomic segments of varying lengths (14,21). This suggests that the molecular mechanism underlying *PLP1* duplication events is likely distinct from the more common NAHR mechanism. We hypothesized that various LCRs in the PMD region might stimulate DNA rearrangements resulting in *PLP1* gene duplication, because complex genomic architecture can cause genomic instability and predispose chromosomal rearrangements (1,2,22) and as LCRs are thought to catalyze non-recurrent rearrangements (23). We therefore performed an extensive bioinformatic analysis of this region and mapped the breakpoints in multiple PMD patients with duplication of *PLP1*. Interestingly, we found that although the duplications differ in size, they appear to cluster into groups of similar size. The rearrangement breakpoints in these groupings appear to be in proximity to unusual genome architecture.

RESULTS

Numerous LCRs identified in the region surrounding *PLP1*

Extensive *in silico* analysis of an ~8 Mb region (Build 35: 98 358 000–106 357 999; Xq22.1-q22.3) uncovered several novel LCRs proximal to *PLP1*, whereas the distal LCRs included only LCR–PMDA through D (Fig. 1). We previously defined the structures LCR–PMDA and B as two inverted repeats, each with two homologous segments: A1a and A2 for LCR–PMDA, and A1b and A3 for LCR–PMDB (18); LCR–PMDC and D were more recently defined by Woodward *et al.* (19) as distal LCRs which flank LCR–PMDA and B. The novel LCRs have greater than 89% identity and are at least 500 bp in length. Compared with similar analyses of the Charcot-Marie-Tooth disease type 1A (4,24), Smith-Magenis syndrome (23,25,26) and Sotos syndrome (27,28) regions, analyses of the *PLP1* region revealed more complex genome architecture, with a greater diversity in the number, copies and orientations of the constituent LCRs surrounding the dosage-sensitive gene *PLP1*.

LCRs with shared homology were discovered only within the 3 Mb region surrounding *PLP1* (Fig. 1). Inter-chromosomal LCRs with homology to regions on various autosomes and chromosome Y, and intra-chromosomal LCRs with homology to other non-adjacent regions on chromosome X were excluded from further analysis. Novel LCRs located ~1.4 Mb proximal to *PLP1*, which we termed LCR–PMDF1 and F2 (Figs 1 and 2, Table 1), represent a set of large LCRs in inverted orientation, each spanning ~122 kb with 99.9% shared sequence identity. LCRs identified nearest to *PLP1* are situated ~276 kb proximal (LCR–PMDE2) and ~125 kb distal (LCR–PMDC) to the gene (Fig. 1, Table 1). Other LCRs in this 3 Mb region (Fig. 1), with their sizes, positions and percent identities, are as shown in Figure 2 and Table 1. There are LCRs in the vicinity of proximal and distal breakpoints of *PLP1* duplications in PMD patients delineated by fluorescence *in situ* hybridization (FISH) mapping (14), including 11 patients reported herein; therefore, we focused on these particular genomic regions for more in-depth analyses of their potential role in *PLP1* duplication events.

Duplication breakpoints are diverse but appear to cluster into groups

In all patients (Table 2) whose *PLP1* duplication has been confirmed by FISH, custom array comparative genomic hybridization (CGH) analysis revealed their duplication sizes at a bacterial artificial chromosome (BAC) and P1 artificial chromosome (PAC) clone resolution (Fig. 3). We detected duplications which covered the span of one or two BAC clones (~180–250 kb), as well as larger duplications (~4–7 Mb), some of which extend distal to *PLP1* beyond the detection range of the array (over 7 Mb). Of the five patients with larger duplications (Table 2), two have cytologically visible duplications by G-banding: BAB2396 [46,XY,dup(X)(q22.1q22.2)] and BAB2425 [46,XX,dup(X)(q22.1q22.3)] (Supplementary Material, Fig. S1). Siblings BAB2389 and 2390 (from family HOU893), have a duplication estimated to be ~4 Mb in size, and their duplication was not cytologically visible; BAB1327 was not analyzed by G-banding.

Interestingly, there appears to be a subgroup of 15 patients (12 families) who have similar proximal and/or distal breakpoints at a BAC/PAC resolution (Figs 3 and 4). This subgroup represents ~71% of our patient cohort (15/21), or 71% of families (12/17), and ~72% of breakpoints (23/32) for the families we report herein. For this subgroup, custom array CGH often revealed four to five BAC clones duplicated (~650 kb), generally including BACs RP11-1123D8, RP11-1144F22, RP11-832L2 (*PLP1*), RP11-34P3 and RP11-462K21 (Fig. 3). Some end clones appear to be partially duplicated because of their intermediate signal intensity, indicating that the breakpoint likely occurs within that particular clone (duplication end clone), whereas others are completely duplicated, suggesting that the breakpoint either occurs within that clone, and/or within the adjacent overlapping clone (duplication end-clone pair).

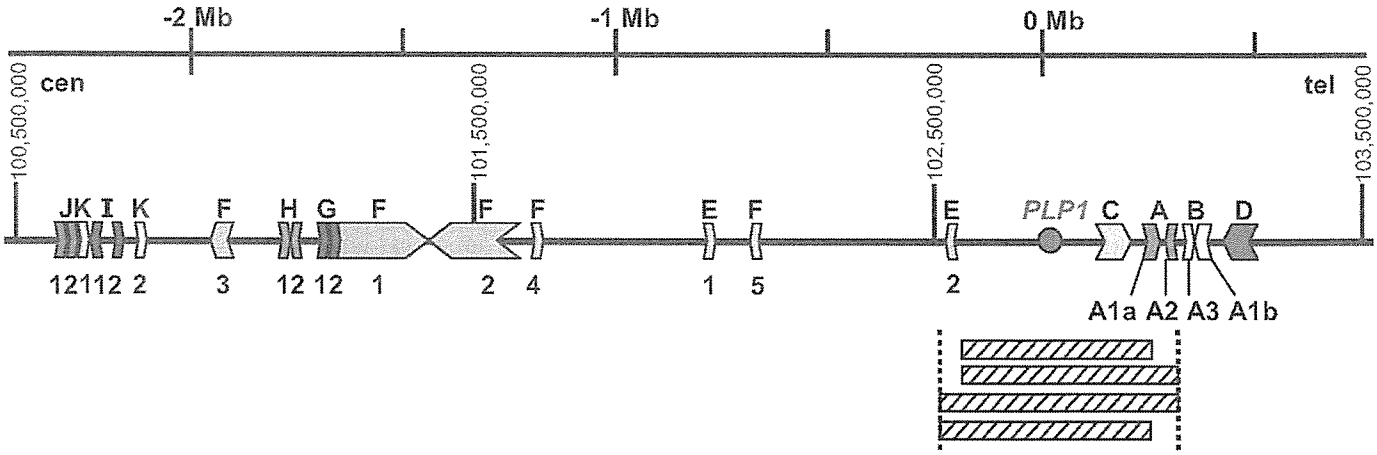

Figure 1. *In silico* analysis reveals LCRs in the 3 Mb region surrounding *PLP1*. Novel LCRs, having pair-wise alignments with greater than 89% identity, are displayed centromeric (cen) to telomeric (tel). Those with shared identity are shown graphically in like colors; the direction of the block arrows indicates the relative orientation. The large orange block arrows, LCR–PMDF1 and F2, contain numerous short subunits and have shared identity in an inverted orientation. The smaller orange LCRs are labeled LCR–PMDF3, F4 and F5; all LCR–PMDFs have shared identity. LCR–PMDG1 and G2 (maroon), LCR–PMDJ1 and J2 (magenta) and LCR–PMDK1 and K2 (pink) are directly oriented LCRs that have shared identity, respectively; LCR–PMDH1 and H2 (brown), LCR–PMDE1 and E2 (light green) and LCR–PMDI1 and I2 (dark purple) are inverted LCRs that have shared identity, respectively. LCR–PMDA (dark blue), LCR–PMDB (light blue), LCR–PMDC (yellow) and LCR–PMDD (dark green) are shown. The *PLP1* gene is indicated by the red circle, and genomic positions are given relative to the *PLP1* gene in megabases. Alignment with representative *PLP1* duplications falling within a subgroup having similar proximal and distal breakpoints is shown (striped bars within vertical dotted lines). The exact size and shared percent identity for these LCRs are given in Table 1 and Figure 2, respectively.

	A1a	A2	A3	A1b	C	D	E1	E2	F1	F2	F3	F4	F5	G1	G2	H1	H2	I1	I2	J1	J2	K1	K2
A1a	100																						
A2	87.8	100																					
A3	89.8	86.8	100																				
A1b	98.9	87.8	89.9	100																			
C					100																		
D					92.7	100																	
E1							100																
E2							95.0	100															
F1									100														
F2									99.9	100													
F3									95.4	95.3	100												
F4									94.2	94.2	94.2	100											
F5									93.4	93.4	93.4	92.9	100										
G1									93.1	93.1				100									
G2									100	99.9				93.1	100								
H1																100							
H2																92.2	100						
I1																		100					
I2																		99.9	100				
J1																				100			
J2																				89.7	100		
K1																						100	
K2																						89.5	100

Figure 2. Grid of cumulative percent identities of all alignments for each LCR–PMD pair. White squares contain percent identity shared among LCRs from horizontal and vertical axes. Grey squares indicate pairs of LCRs which have no significant indentity.

Breakpoint groupings are coincident with complex architecture

After determining which of the custom array CGH clones contain LCRs (Table 1), we sought to determine if the breakpoints of the above subgroup of PMD patients who appear to have similar proximal and/or distal breakpoints at a BAC/PAC resolution (Figs 3 and 4) occur within or near LCR-containing clones to test the hypothesis that LCR–PMDs are stimulating, but not necessarily mediating, these rearrangements. From this analysis, we identified the following LCR-containing clones at or near the breakpoints: RP11-1123D8 (LCR–PMDE2),

Table 1. LCR–PMDs from previous and present *in silico* analyses

LCR–PMD	BAC(s) within	Size (kb)	Position (Build 35)	Orientation
AA1a	*RP11-462K21*	18.5	103,029,820-103,048,307	(+)
AA2	*RP11-462K21*	10.3	103,064,260-103,074,533	(−)
BA3	*RP11-462K21*	13.9	103,096,154-103,110,142	(+)
BA1b	*RP11-462K21*	18.5	103,111,984-103,130,746	(−)
C	*RP11-34P3*	34.8	102,978,791-103,013,644	(+)
D	*RP11-462K21*	26.9	103,137,452-103,164,433	(−)
E1	RP11-155E24	2.4	101,998,037-102,000,480	(+)
E2	*RP11-1123D8*	2.4	102,559,737-102,562,186	(−)
F1	RP11-461E24	121.9	101,276-701-101,398,620	(+)
F2	RP11-669M24	121.9	101,410,623-101,532,603	(−)
F3	CTD-2006G2	8.4	100,898,811-100,907,221	(−)
F4	CTD-2131P19	1.4	101,625,289-101,626,682	(+)
F5	RP11-1061F13	1.3	102,141,897-102,143,193	(−)
G1	RP11-165B8, RP11-461C20	11.3	101,234,198-101,245,515	(+)
G2	RP11-461C20	4.8	101,282,660-101,287,458	(+)
H1	RP11-165B8	0.9	101,187,082-101,187,979	(+)
H2	RP11-165B8	0.9	101,202,419-101,203,313	(−)
I1	RP11-66I17	4.5	100,658,634-100,663,108	(−)
I2	RP11-66I17	4.5	100,672,941-100,677,415	(+)
J1	RP11-15E22	0.7	100,557,050-100,557,755	(+)
J2	RP11-15E22	0.7	100,615,928-100,616,623	(+)
K1	RP11-15E22	0.6	100,621,785-100,622,389	(+)
K2	RP11-15E22	0.7	100,689,999-100,690,668	(+)

LCR-containing BAC clones listed are from those on our CGH array. Sets of LCRs are designated by LCR-PMD letter, with the following previously published exceptions: *A* and *B* are a set of four LCRs (18), and *C* and *D* are a set of two LCRs (19). Relative orientation within each set of related LCRs assigned as (+) or (−). LCRs and BACs in italics are those which are present at/near the breakpoints in a subset of patients with similar breakpoints at a BAC/PAC resolution.

Table 2. Cohort of patients included in the present study

Family (HOU#)	Patient (BAB#)	Sex
485	1258[d]	M
487	1263[a,d]	M
	1264[a,d]	M
587	1482[b]	M
	1597[b]	M
519	1334[d]	M
674	1705[a]	M
	1707[a]	M
503	1305[d]	M
501	1301[d]	M
944	2448[c]	M
486	1261[d]	M
494	1282[d]	M
491	1275[d]	M
497	1290[d]	M
561	1420	M
893	2389[a,c]	M
	2390[a,c]	M
924	2396[c]	M
516	1327[c,d]	M
936	2425[c]	F

[a]Siblings within the same family, as listed by HOU#.
[b]Cousins within the same family.
[c]Larger duplication patients (at least ~4 Mb).
[d]Clinical details previously published (14).
[e]Clinical details previously published (47).

RP11-34P3 (LCR–PMDC) and RP11-462K21 (LCR–PMDA, B, and D), which range from 132 to 192 kb in length (average being 146.5 kb). The latter clone is also found at the distal breakpoint for some larger-sized *PLP1* duplications. In a BLAST 2 analysis of the individual breakpoint-spanning clones (Fig. 3), we did not find any additional stretches of >200 bp that shared >85% identity.

We calculated the number of breakpoints that occur within an LCR-containing BAC or PAC duplication end clone or duplication end-clone pairs, versus the number of breakpoints that occur within non-LCR clones. Considering only families with at least one similar breakpoint, we determined that 92% of proximal breakpoints (11/12) and 92% of distal breakpoints (11/12) occur within LCR-containing duplication end clones or duplication end-clone pairs. Considering both proximal and distal breakpoints together, 92% of the breakpoints (22/24) occur within LCR-containing duplication end clones or duplication end-clone pairs for this subgroup. Analyzing the aggregate data from all families in our cohort, 71% of proximal breakpoints (12/17) and 87% of distal breakpoints (13/15) occur in an LCR-containing end clone or end-clone pair. We included only 15 total distal breakpoints (and 32 total breakpoints) because the duplications in two patients (BAB2396 and 2425; Fig. 3) extend distally beyond the genomic region detected by our custom array.

On our array, 14 of the 68 tiled BAC and PAC clones contain LCR–PMDs (Table 1). When we compared the frequency of families with at least one breakpoint in an LCR-containing end clone or end-clone pair ($12/17 = 0.7059$) with the frequency of LCR-containing clones on the full-length array ($14/68 = 0.2059$), the observed frequency is significantly higher, with a P-value of 1.255×10^{-5}. The P-value was determined by performing a binomial test of the proportion

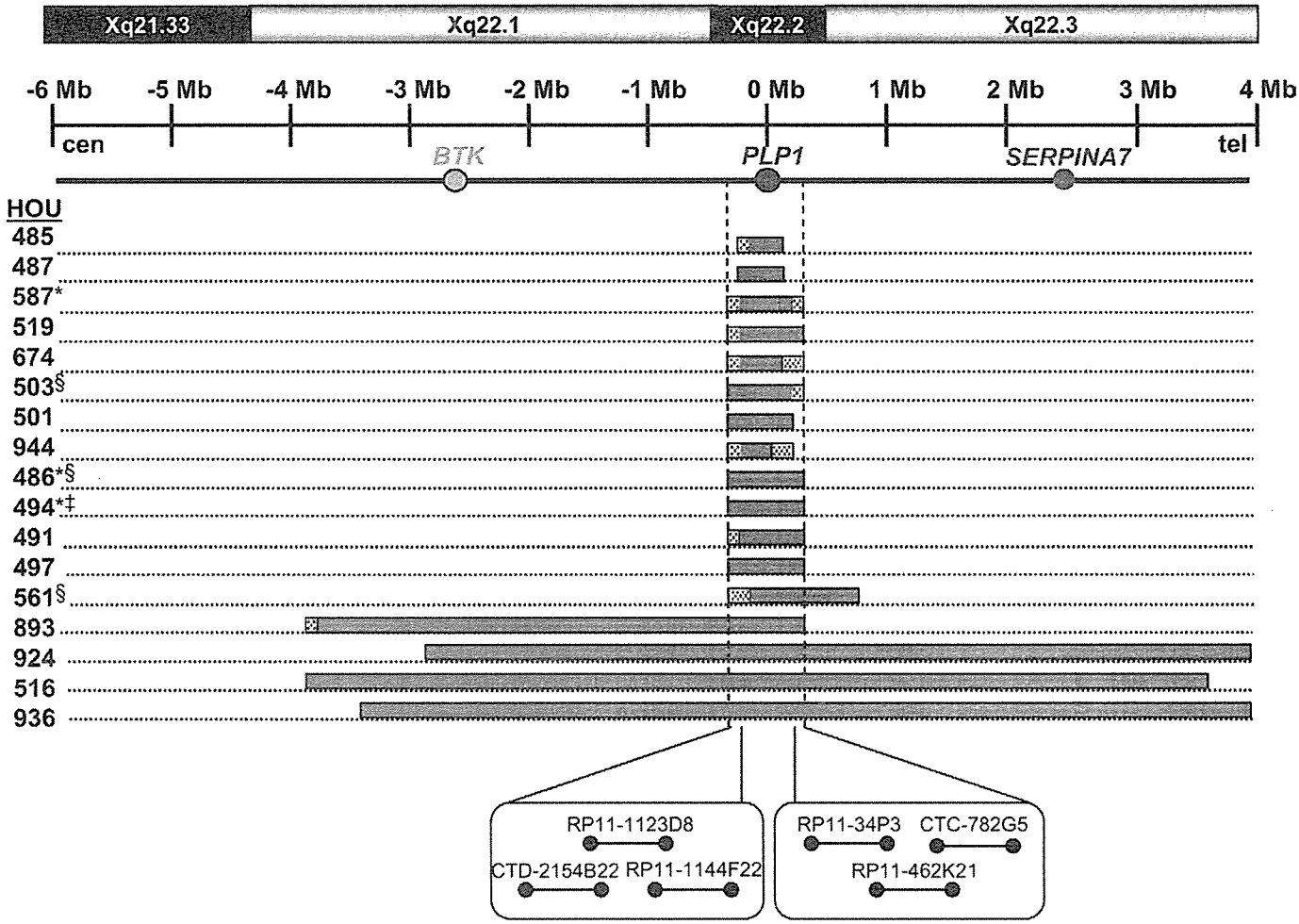

Figure 3. Genomic regions duplicated in our cohort of PMD families analyzed by array CGH. Note the grouping of breakpoints in a subset of patients, delineated by vertical dotted lines; graphical normalized data for these patients are displayed in this figure. Duplication regions similar at a BAC/PAC resolution generally include BAC clones RP11-1123D8, RP11-1144F22, RP11-832L2, RP11-34P3 and RP11-462K21; RP11-832L2 contains the full-length *PLP1* gene. Patients in families HOU924 and 936 have large duplications that extend beyond the region detected by the ~10 Mb array. Representative data for each family are listed by HOU#; those denoted by an asterisk are further discussed in Figure 6; those denoted by a section symbol are complex rearrangements; and that denoted by a dagger symbol is an interrupted direct duplication. Solid blue bars represent clones for which the mean normalized $\log_2$(Cy3/Cy5) ratio of the CGH signal reached a threshold of at least 0.2, except for families HOU501, 516 and 936 for which the ratio approached the threshold yet still represent copy number gains; their duplication sizes were confirmed independently by FISH. Checkered blue bars represent partially duplicated end clones. The boxes below highlight duplication end clones (including single end clones and end-clone pairs) found at the duplication breakpoints. Positions are given relative to the *PLP1* gene (red circle) in megabases, centromeric (cen) to telomeric (tel), and the chromosomal band position is shown on top in alternating black and gray bars. *BTK* and *SERPINA7* genes are shown as green and blue circles, respectively, as a reference.

of observed breakpoints in LCR-containing end clones or end-clone pairs, and the *P*-value is exact.

Probes adjacent to LCRs detect junction fragments

To further investigate whether these LCRs may stimulate the genomic rearrangements resulting in *PLP1* duplication, we examined for an association between breakpoint genomic position and co-localization of an LCR. For this, we employed pulsed-field gel electrophoresis (PFGE) analysis followed by hybridization with a series of DNA probes complementary to unique sequences adjacent to LCRs neighboring *PLP1* (Fig. 5). We examined 15 families in this analysis with two different endonuclease digestions and up to 10 different hybridization probes, which resulted in multiple independent hybridizations per family and a scan that covers a total of ~2 Mb spanning the *PLP1* genomic region. We detected recombination-specific junction fragments in 12 patients in 10 families (Table 3). Similar sized junction fragments, within ~100 kb in size, were observed in eight of 10 families. For example, for hybridization with Distal A probe after *Pme*I digestion, 375 kb junction fragments were observed for families HOU587 and 519; 295 kb junction fragments were observed for families HOU674, 503, 497 and 561; 275 kb junction fragments were observed for families HOU486 and 494 (Table 3). In four patients from three families for which complete restriction mapping by PFGE was possible (Fig. 6), we mapped both the proximal and distal ends of

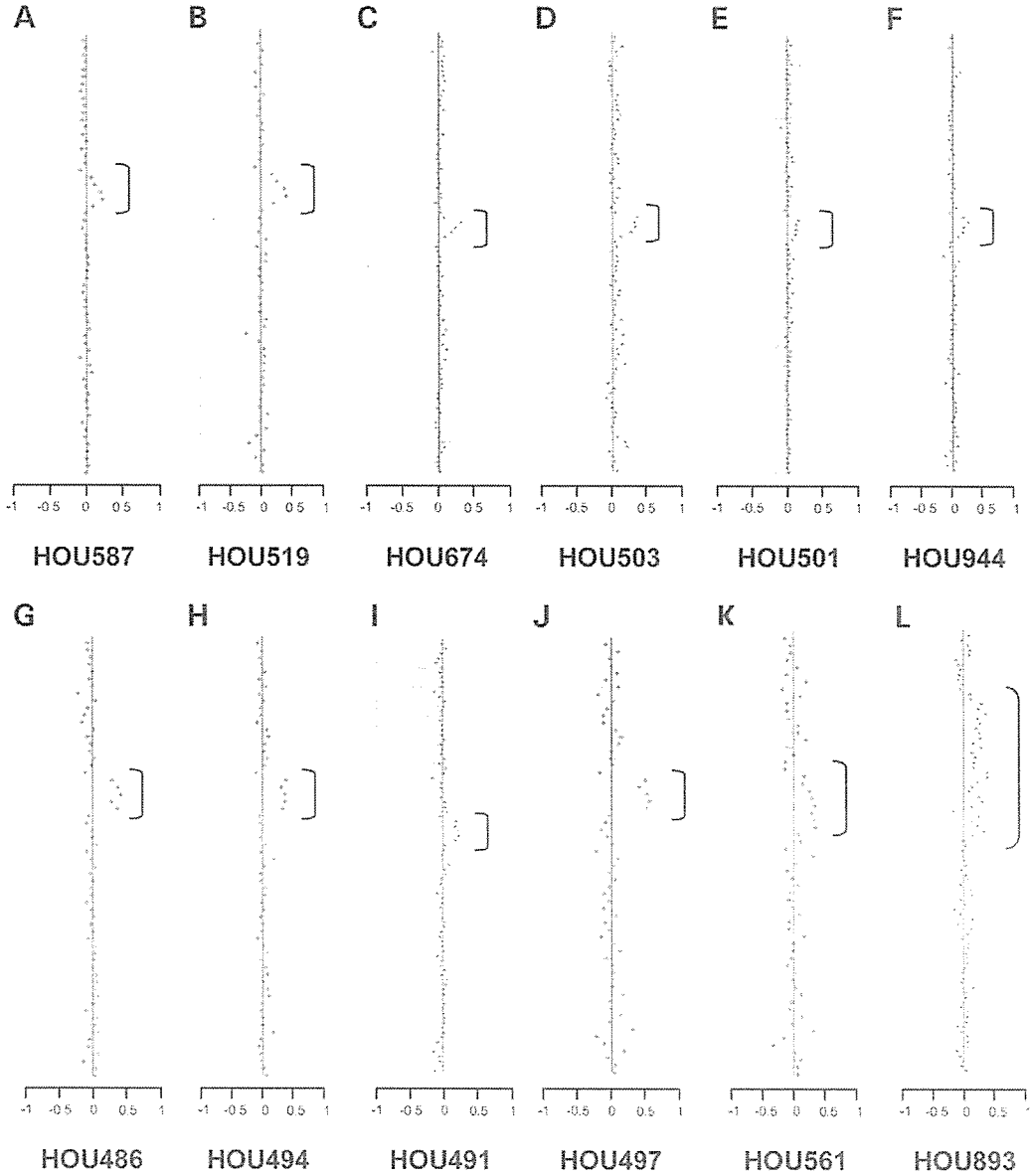

Figure 4. Similar clones duplicated in several PMD patients. Normalized array CGH data for families HOU587, 519, 674, 503, 501, 944, 486, 494, 491, 497, 561 and 893, who have at least one similar breakpoint at a BAC/PAC resolution, are displayed in (A–L), respectively. For families with more than one affected individual, representative data for only one individual is displayed. As expected, patients in these families appear to have similar proximal and/or distal breakpoints at a BAC/PAC clone resolution. Duplicated regions are indicated by the brackets to the right of each vertical axis. Data from our 38 clone array are displayed in (A, B, G, H, J and K); data from our 68 clone array are displayed in (C–F, I and L).

the *PLP1* duplications. Of all the hybridization probes tested, only Proximal A, B, C, G and Distal A probes identified junction fragments. Distal Probe A is located just proximal to LCR–PMDA (Fig. 5).

For family HOU587, as anticipated, we observed segregation of the junction fragment for all affected and carrier family members, whereas the unaffected male BAB1754 showed only the expected normal band (Fig. 6). Hybridization with Proximal G probe and Distal A probe yielded junction fragments after both *Pme*I and *Nru*I enzyme digestions, whereas hybridization with Proximal C probe yielded junction fragments after *Nru*I digestion. In all junction-positive members of family HOU587, the junction fragments were larger than the expected band sizes, indicating that for the junction fragment, the restriction enzyme sites flanking the hybridization probe are further apart than on non-rearranged DNA (Fig. 5). By restriction enzyme mapping and comparative analysis with reference genome sequence, the duplication is in tandem and is direct in orientation.

In families HOU486 and HOU494, hybridization with Proximal C and Distal A probes yielded junction fragments after *Pme*I digestion, and with Proximal C and G and Distal A probes after *Nru*I digestion. We observed junction fragments of larger than normal-sized bands expected based on restriction maps (Fig. 5) after *Pme*I digestion as described earlier for family HOU587, but of smaller size than the

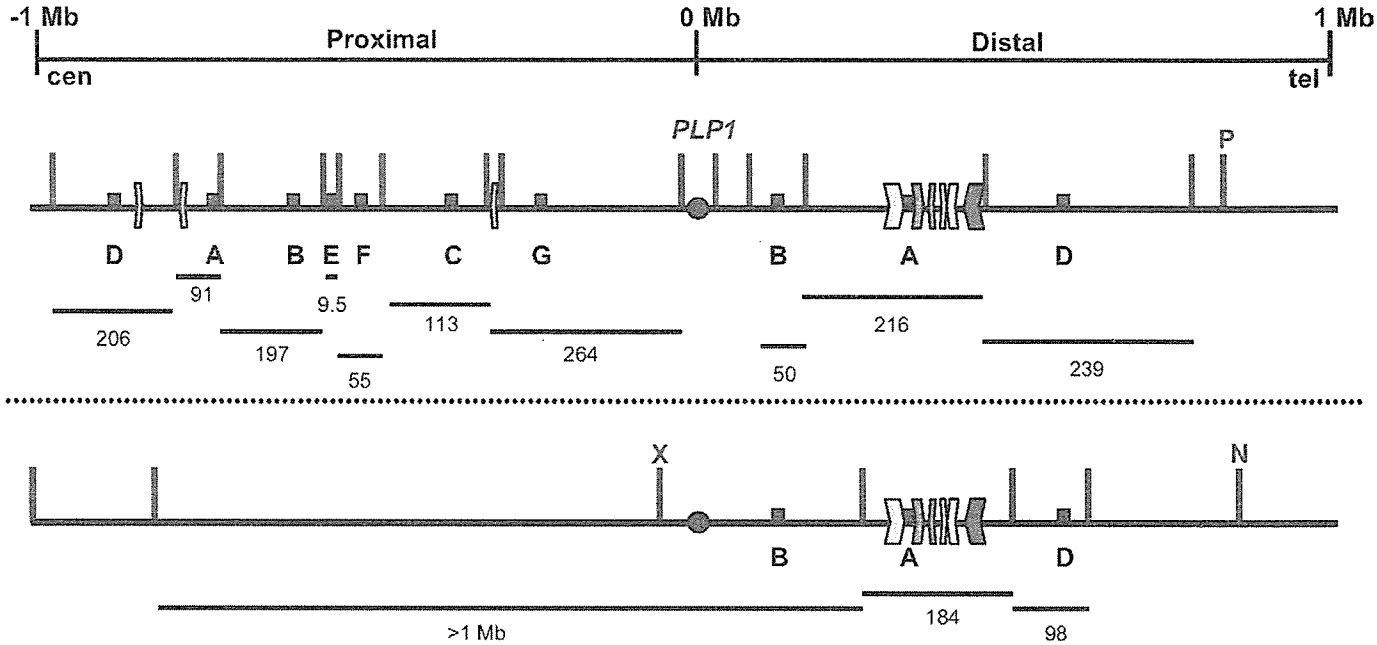

Figure 5. Probes adjacent to LCRs detect apparent junction fragments. Block arrows proximal to *PLP1* (red circle) centromeric (cen) to telomeric (tel) represent LCR–PMDE1, F5 and E2, respectively, which were identified by large-scale genome sequence analysis as described. Block arrows distal to *PLP1* include LCR–PMDA and B in dark blue and light blue, respectively, which are flanked by LCR–PMDC (yellow) and LCR–PMDD (dark green). Proximal A through G probes were designed proximal to *PLP1*, whereas the Distal A, B and D probes were designed distal to *PLP1*. The positions where probes hybridize are shown as small red squares. The upper and lower panels depict the restriction maps for enzymes *Pme*I, 'P,' and *Nru*I, 'N,' respectively. The expected band sizes by Southern hybridization with a particular probe and restriction enzyme combination are specified in kilobases below each restriction map. 'X' indicates that *Nru*I does not cut at the expected site, likely because of its CpG methylation sensitivity. Positions are given relative to the *PLP1* gene in megabases.

Table 3. Summary of band sizes (in kb) observed for *PLP1* duplication patients tested for hybridization with Proximal B, C, and G and Distal A probes

Family	Patient	Proximal B probe		Proximal C probe		Proximal G probe		Distal A probe	
		*Pme*I	*Nru*I	*Pme*I	*Nru*I	*Pme*I	*Nru*I	*Pme*I	*Nru*I
HOU587	BAB1482	197	ND	113,136	*480*	264,*375*	*480*	216,*375*	184,*480*
	BAB1597	197	ND	113,136	*480*	264,*375*	*480*	216,*375*	184,*480*
HOU519	BAB1334	197	ND	113,136	ND	264	ND	216,*375*	184
HOU674	BAB1705	197	ND	ND	ND	264	ND	216,*295*	184,*400*
	BAB1707	197	ND	ND	ND	264	ND	216,*295*	184,*400*
HOU503	BAB1305	197	ND	113,136	ND	264	ND	*295*	*100*
HOU501	BAB1301	197	ND	113,136,*190*	ND	264	ND	216	ND
HOU486	BAB1261	197	ND	113, 115,*127*,136	*650*	264	*650*	*275*	*100*
HOU494	BAB1282	197	ND	*90*,113,*115*,136	*650*	264	*650*	216,*275*	*100*,184
HOU491	BAB1275	197,*210*	ND	113,136	ND	264	ND	216	ND
HOU497	BAB1290	197	ND	113,136	ND	264	ND	216,*295*	*100*,184
HOU561	BAB1420	197	ND	ND	ND	264	ND	*295*	*100*

Hybridization with all other probes in the probe series yielded expected band sizes. Band sizes in italics indicate approximate junction fragment lengths; all others indicate observed bands of expected sizes. 'ND' signifies not determined. All band sizes listed are estimated based on migration with a yeast or lambda DNA size marker.

normal bands after *Nru*I digestion, indicating that for the junction fragment, the *Nru*I sites flanking the hybridization probe are closer together than on non-rearranged DNA. By restriction analysis for family HOU494, the duplication is consistent with being directly oriented, but appears to be interrupted, and inserted nearby the original reference sequence. Interestingly, we observed the absence of bands of expected sizes based on restriction maps in family HOU486, and also in families HOU503 and 561, and instead saw junction fragments only, suggesting that more complex rearrangements have occurred, and that more than one breakpoint may have occurred within the same restriction fragment. For families HOU486 (BAB1261) and HOU503 (BAB1305), the distal breakpoints determined by PFGE align with that found by array CGH analysis. However, for family HOU561 (BAB1420), array CGH analysis detected a duplication that extends three more BAC clones (~500 kb) distal to that predicted by PFGE analysis, also consistent with a complex rearrangement. We detected no bands for family member BAB1698 (HOU486) for hybridization with

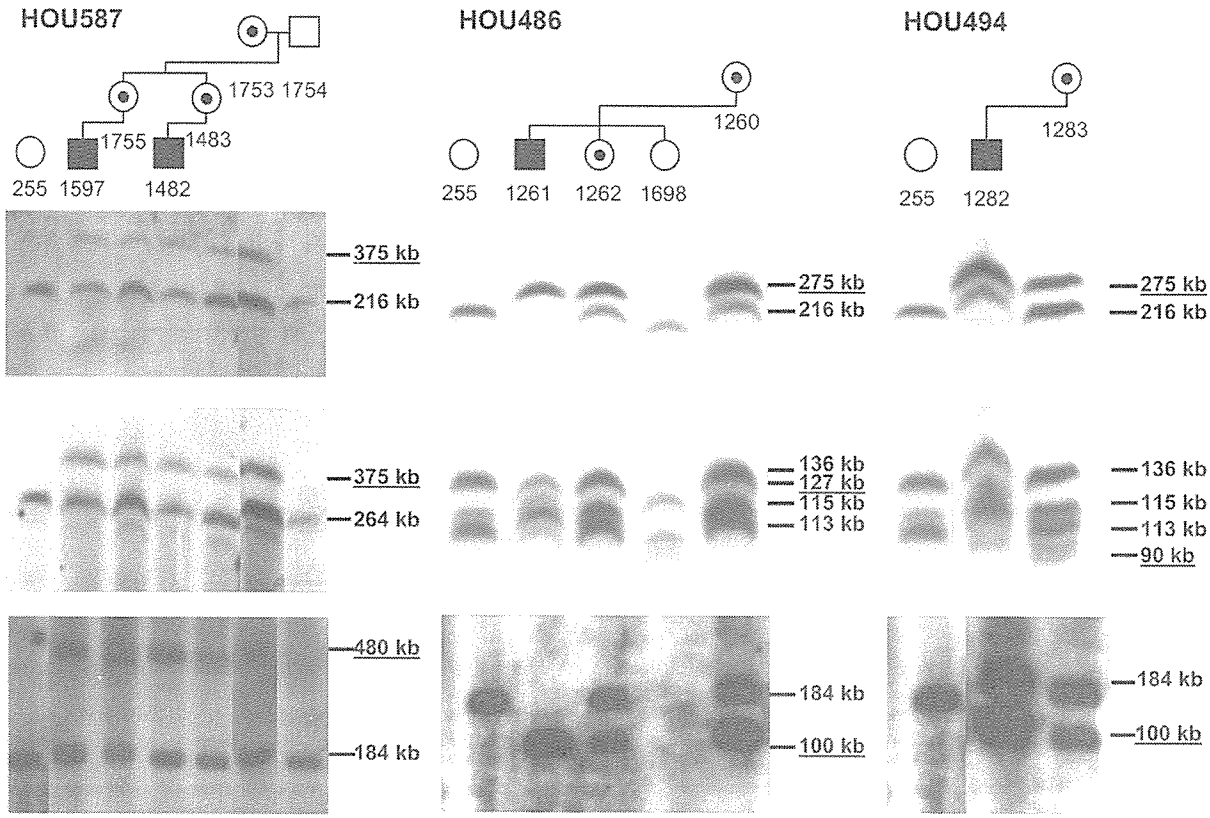

Figure 6. Junction fragments segregate in families. Shown are the PFGE data for *Pme*I and *Nru*I digestions. Family HOU587 is shown on the left, family HOU486 in the center and family HOU494 on the right. Hybridization with Distal A probe after *Pme*I digestion is shown in the first row, and after *Nru*I digestion in the last row for all three families. In the second row, hybridization with Proximal G probe after *Pme*I digestion is shown for family HOU587, whereas hybridization with Proximal C probe after *Pme*I digestion is shown for families HOU486 and 494. Approximate band sizes are shown in kilobases to the right of each blot. Junction fragments (band sizes underlined) are identified as bands of sizes differing from those observed for the control individual (BAB255).

the Distal A probe after *Nru*I digestion, which is possibly due to mutation affecting the *Nru*I restriction pattern in this individual, as bands are otherwise able to be visualized by hybridization with other probes. A summary of the results of our PFGE analysis of patients in families HOU587, 486 and 494 is illustrated in Figure 7, highlighting LCR–PMDE2 found adjacent to where Proximal C and G probes hybridize, and LCR–PMDA found adjacent to where Distal A probe hybridizes.

Diverse duplication breakpoints with grouping near complex genomic architecture supported by recombinant junction analysis

Earlier, we showed by array CGH that duplications have diverse breakpoints, but that they occur in groups coincident with LCRs. Furthermore, in a prospective approach, we used unique sequence probes adjacent to LCRs in Southern analysis, after separation of high molecular weight genomic DNA by PFGE, to detect junction fragments associated with the rearrangement breakpoints. To examine an independent data set to determine whether or not there was any evidence for grouping among the diverse breakpoints, we utilized the recently published PMD duplication recombinant junction sequence analysis by Woodward *et al.* (19). This enabled us to position *PLP1* duplication breakpoints precisely on the X chromosome genomic sequence to examine for breakpoint grouping and potential association with LCRs. Indeed, we found an apparent grouping of breakpoints coincident with LCRs (Fig. 8). In fact, ~62% of the proximal breakpoints (8/13) and ~79% of the distal breakpoints (11/14; one patient has two sequenced distal breakpoints) occur within or near LCR-containing BAC clones. Overall, ~77% of patients (10/13) in their data set had at least one breakpoint within or near an LCR-containing BAC clone. In common, with our subset of patients with at least similar breakpoints at a BAC/PAC resolution, the proximal breakpoints of their data set (6/13 patients) occurred within or near BAC clone RP11-1123D8 (LCR–PMDE2), and the distal breakpoints of their data set (9/13 patients and 3/13 patients) occurred within or near BAC clones RP11-34P3 (LCR–PMDC) and RP11-462K21 (LCR–PMDA, B, and D), respectively. In addition, two of their patients had proximal breakpoints within or near BAC clone RP11-155E24 (LCR–PMDE1).

The duplications are directly oriented

The PFGE restriction patterns we observed for families HOU486, 503 and 561 prompted us to investigate duplication orientations in all available patients. Two-color FISH analysis

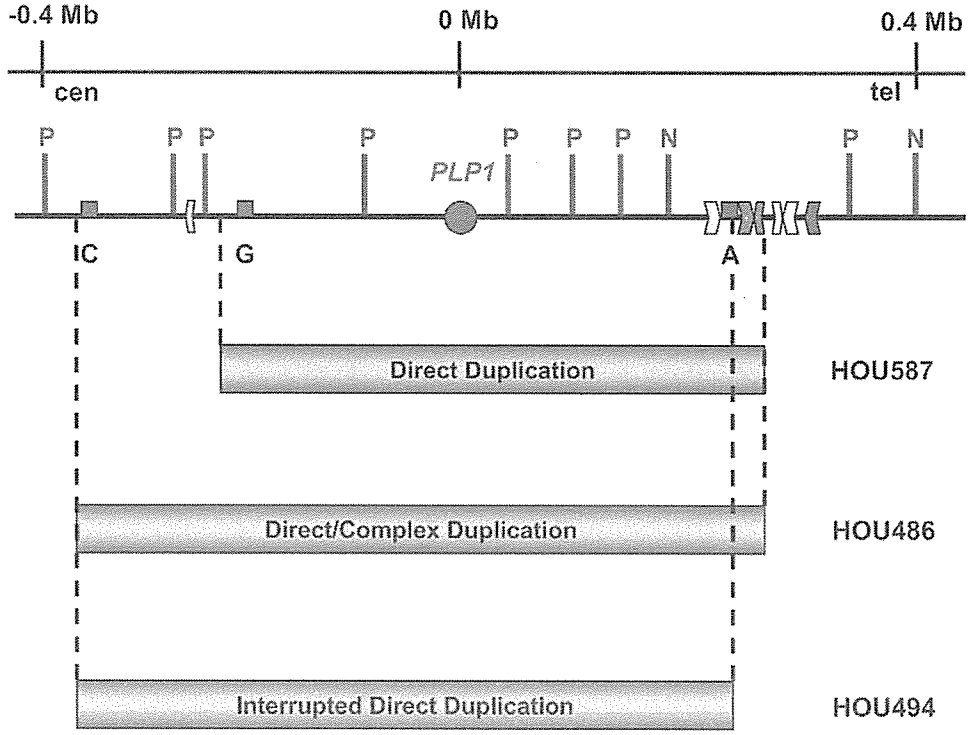

Figure 7. PFGE junctions map breakpoints near LCRs. Summary view of *PLP1* duplications found in families HOU587, 486 and 494 by PFGE analysis; duplications are shown as pink horizontal bars. Positions of the Southern hybridization probes (red squares) relative to the LCR–PMDs most nearby the duplicated regions are indicated. LCR–PMDE2 (light green) is the nearest LCR adjacent to Proximal C and G probes (~31 and ~33 kb away, respectively). LCR–PMDA (dark blue), B (light blue), C (yellow) and D (dark green) are shown distal to *PLP1* (red circle). LCR–PMDA is the nearest LCR to Distal A probe (<20 bp away). Restriction sites for *Pme*I digestion are shown as 'P' (purple) and for *Nru*I as 'N' (blue). The approximate endpoints of the duplications are specified by the dashed lines. Duplications are displayed for each family as direct, direct/complex and interrupted direct.

for each patient revealed an alternating red-green-red-green signal order consistent with directly oriented duplications in patients BAB1305, 1301, 1261, 1282, 1275, 1290, 1420, 2389, 2390, 2396 and 2425, as had been observed previously (14). For patients BAB1482, 1597, 1334, 1705 and 1707, the furthest duplicated clones, RP11-1144F22 and RP11-34P3, had only 51 kb of genomic sequence between them, and thus the fluorescent signals could not be reliably distinguished by interphase FISH. Representative data for the direct duplications are shown in Figure 9. For all unaffected male and female control chromosomes, we observed only a red-green signal pattern (data not shown).

No evidence for an association with copy-number variation in LCR–PMDA and B region

We previously identified copy-number variation (CNV) within the LCR–PMDA and B region within a Caucasian control population by a quantitative real-time PCR assay (29). We sought to determine if our PMD patients or family members have CNV in this region in order to investigate CNV as a potential further genomic susceptibility factor for rearrangements. Using the same quantitative real-time PCR assay (29), we evaluated all available PMD patients and family members for CNV in the LCR–PMDA and B region. The results of our dosage assay (data not shown) were consistent only with either *PLP1* duplication or duplication carrier status, and were consistent between patient and mother, as determined previously by FISH and PFGE analyses. Thus, there was no evidence for CNV in the interrogated region in this cohort of patients and family members. These real-time PCR results were also informative for breakpoint analysis in some patients, allowing us to either include or exclude the interrogated region as duplicated or not duplicated, respectively (data not shown).

DISCUSSION

PLP1 duplications causing PMD have been reported as varying in size with scattered breakpoints and lack of homology reported at the actual breakpoints (14,30). For both *PLP1* deletions and duplications causing PMD, recombinant junction sequence analysis revealed a lack of homology and the addition of nucleotides at the breakpoints, consistent with recombination occurring by an NHEJ mechanism (18,19,31). Moreover, NHEJ has been implicated recently as an alternative mechanism responsible for a number of human genomic disorders because of non-recurrent rearrangements with scattered breakpoints (22,23,32). On the basis of the following observations, we suggest that the LCRs not only render this genomic region unstable and susceptible to

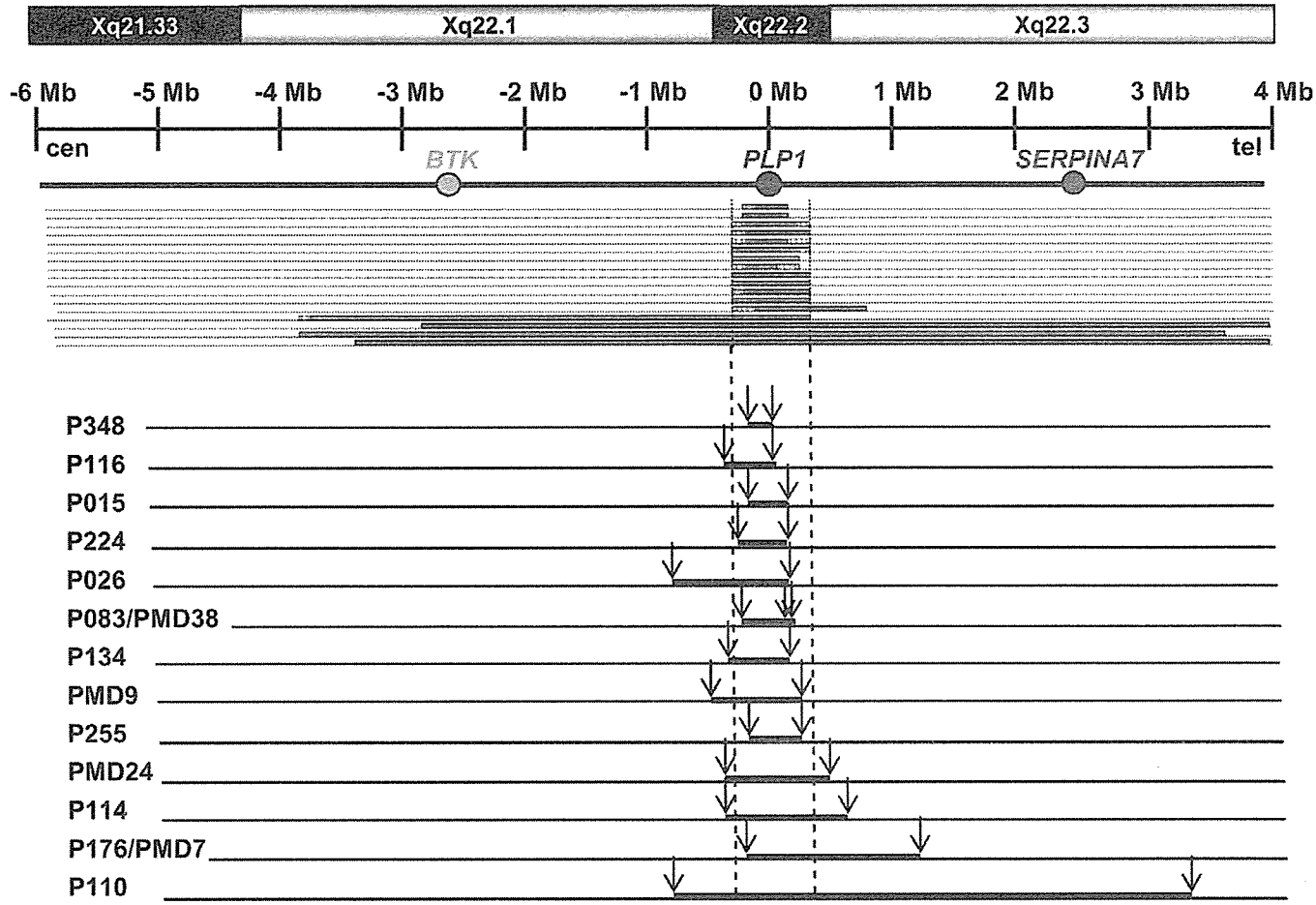

Figure 8. Comparative analysis of an independent data set (19) reveals apparent grouping of breakpoints. The region detected by array CGH is shown on the top, followed by the duplications found in our patients by array CGH in condensed form (Fig. 3). Below are the duplications reported by Woodward *et al.*, and their alignment within our ~10 Mb array detection region. For this independent data set, patients are shown on the left; duplication breakpoints are shown as vertical arrows, whereas the duplicated segments are shown as bold black lines between the arrows. Similar breakpoint regions in a subset of our patients are delineated by vertical dotted lines.

rearrangements, but that they are in fact, stimulating these genomic rearrangements.

Genomic architecture of the *PLP1* region is complex

By *in silico* genome sequence analysis, there is no gap in sequence information between LCR–PMDA and B, unlike what we previously published based on the then current draft sequence information. According to our FISH mapping data (14), the distal breakpoint ends of *PLP1* duplications in most *PLP1* duplication families tested grouped at or near LCR–PMDA and B, a complex arrangement of four LCRs of varying shared sequence identities and different relative orientations (Figs 1 and 2; Table 1), whereas the proximal breakpoints were more scattered. These data prompted us to perform an extensive *in silico* genome sequence analysis described herein that uncovered many LCRs scattered proximal to *PLP1*, and fewer distal to *PLP1*. Interestingly, the locations of scattered LCRs within 2.3 Mb of sequence proximal to *PLP1* correlates with the scattered proximal breakpoints previously reported in *PLP1* duplication patients, and the clustering of LCRs distal to *PLP1* correlates with the grouped distal breakpoints previously reported (Fig. 1).

LCR–PMDs are associated with duplication breakpoints in a subset of patients

Although duplication breakpoints proximal to *PLP1* have been shown to be scattered, array CGH analysis on our cohort of *PLP1* duplication patients surprisingly revealed that there is a subgroup of duplication patients who have similar proximal and/or distal breakpoints at a BAC/PAC resolution (Figs 3 and 4), accounting for ~71% of our patient cohort (15/21) or 71% of families (12/17). Furthermore, when our array CGH breakpoint mapping data were aligned with LCR data generated from *in silico* analysis, we found that the breakpoints in 12 families aligned with the locations of LCR–PMDs with statistical significance

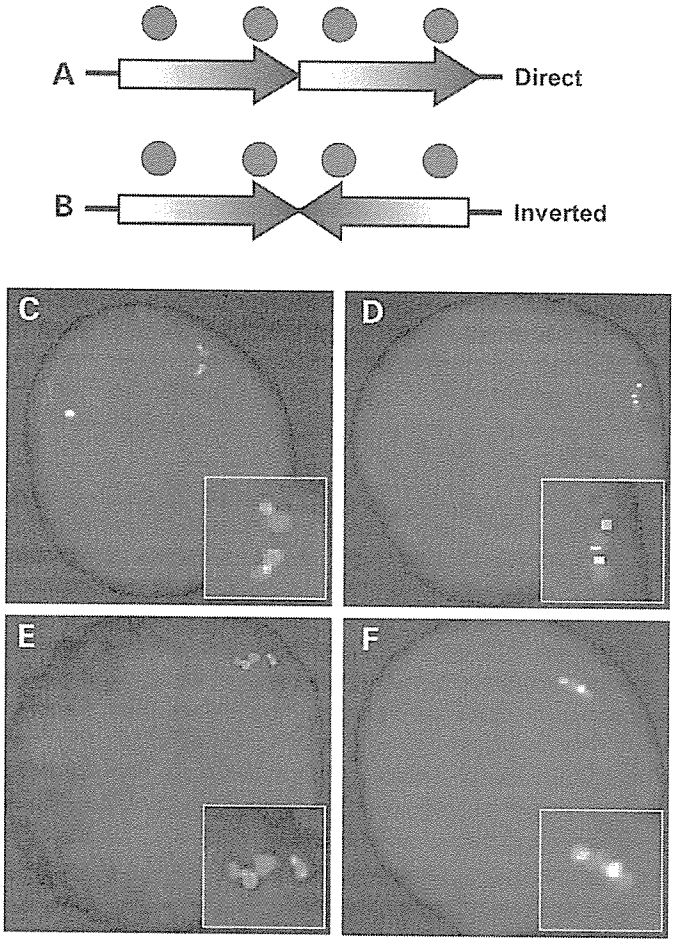

Figure 9. FISH showed direct orientation of duplications. Representative data for two-color FISH analysis for duplication orientation are shown. The signal order is shown as (**A**), red-green-red-green for direct duplication and (**B**), red-green-green-red for inverted duplication. The BAC probe labeled in red is the most proximal fully duplicated clone (if available), whereas the BAC probe labeled in green is the most distal fully duplicated clone (if available) as shown by array CGH. (**C**) shows a representative analysis of the mother of a male duplication patient, whereas (**D**–**F**) show representative orientation analyses of unrelated male duplication patients. Enlargements of the duplicated segments are shown in each respective insert. These data are typical results for the direct duplications we observed.

($P = 1.255 \times 10^{-5}$). In fact, for this subgroup, we found that 92% of their proximal breakpoints and 92% of their distal breakpoints occur within LCR-containing BAC clones or duplication end-clone pairs.

By PFGE analysis, we were able to confirm that the LCRs in the *PLP1* region are associated with breakpoints of duplications causing PMD. Using probes that map in proximity to LCRs and target suspected proximal and distal breakpoint regions, we identified junction fragments in 12 patients in 10 families; in four of them, junction fragments were identified on both the proximal and distal ends of the duplicated segments. These four patients are included in the subgroup of patients who have similar proximal and distal breakpoints at a BAC/PAC resolution. The Distal A hybridization probe, designed adjacent to LCR–PMDA and B, detected distal junction fragments in the majority of patients tested, whereas multiple hybridization probes mapping proximal to *PLP1* were informative, consistent with the pattern of LCRs we find in this region. In other words, a majority of distal breakpoints occur near or within LCR–PMDA and B in our patients, whereas the proximal breakpoints occur near various LCR–PMDs. Junction fragments could not be resolved for patients with particularly large or small duplications under the separation conditions and by the restriction enzymes used. In addition, if a duplication proximal breakpoint occurred within LCR–PMDE2 or within the 9.5 kb between the *Pme*I sites flanking LCR–PMDE2, the resulting junction fragment would only be able to be detected after *Nru*I digestion, unless conventional Southern analysis were performed. Our PFGE data presented herein suggest an association between breakpoints and proximal and distal LCRs, implicating genome architecture in the rearrangement events leading to *PLP1* duplications in some PMD patients.

Moreover, when we investigated the potential grouping of breakpoints in an independent data set published by Woodward *et al.*, in which recombinant junctions were sequenced (19), we also found that indeed a majority (10/13) of their patients had at least one breakpoint within or near LCR-containing BAC clones. In particular, similar to the findings reported herein, we found an association between LCR–PMDE1 and E2 and proximal breakpoints, and between LCR–PMDA, B, C, and D and distal breakpoints in their data set.

PLP1 duplications may share a common mechanism

PLP1 duplications resulting in PMD generally occur in tandem by an intra-chromosomal event in an ancestral male during gametogenesis (14,21,33). Intra-chromosomal events having occurred in an ancestral male are also responsible for duplications causing Duchenne muscular dystrophy (34) and *PLP1* deletions (18).

In analyzing PFGE data, the placement of hybridization probes relative to the restriction sites can be informative for determining breakpoint locations of rearrangements (35). By PFGE analysis, we observed similar size-junction fragments for some unrelated patients, possibly indicating that they share a common breakpoint region, or at least that the breakpoints occur within a similar genomic vicinity. Our array CGH analysis revealed that the breakpoints are indeed similar for a subset of patients. Also, our restriction analysis by PFGE showed that the rearrangements in some of our patients are consistent with directly oriented duplications. Likewise, our two-color FISH analysis revealed that the duplications in all patients tested were direct in orientation. The commonalities observed in the junction fragment sizes, breakpoint locations and duplication orientations suggest that a common mechanism may be responsible for the duplication rearrangements in these patients.

The *PLP1* region is prone to rearrangement

Not only have patients with PMD resulting from *PLP1* duplication, deletion or point mutations been described, but other DNA rearrangements have also been shown to be causative. PMD cases in which *PLP1* has behaved as a sub-microscopic

transposon have been reported (30,36), including one in which all the genetic material including the centromere was inverted between two intact *PLP1* copies (30). Whether inversions are the cause of such duplications, or if duplications have led to these inversions by mispairing is difficult to determine. In addition, extra copies of *PLP1* have been reported to be found on some autosomes (18,37). Interestingly, in some patients, three or more copies of *PLP1* have been reported (38), including partial triplications and partial deletions as well (39). We report herein at least one patient (BAB1282) with an interrupted direct duplication, and at least three patients (BAB1305, 1261, 1420) with potentially complex duplication rearrangements as shown by the absence of normal-sized bands by PFGE analysis, one of which (BAB1420) has a duplication detected by array CGH that extends three more BAC clones (~500 kb) distal to that predicted by PFGE analysis. Considering that the region surrounding *PLP1* contains numerous LCRs based on *in silico* analysis reported herein, and that repeat sequence confers genome instability (1,40), the genomic architecture likely renders the DNA in this region highly susceptible to duplication and other rearrangements causing PMD.

Particular LCR–PMDs may be hotspots for stimulating *PLP1* duplications

It appears that the region containing LCR–PMDA and B is possibly a hotspot for stimulating rearrangements (18), including those leading to CNV of the LCR–PMDA and B region in normal individuals as we recently described (29). CNV in the LCR–PMDA and B region was excluded in this study, in all available PMD patients and family members. Besides LCR–PMDA and B, LCR–PMDE2, which is the closest LCR proximal to the *PLP1* gene and is adjacent to PFGE Proximal C and G probes (Fig. 5), may also play a role in stimulating *PLP1* duplication events, as we report rearrangement proximal breakpoints having occurred near this sequence. Therefore, we suggest that rearrangements stimulated by both of these particular LCR regions together, proximally and distally, in the same event result in duplications of relatively similar size in some patients. Likewise, other pairs of LCRs in this region may stimulate rearrangement together, proximally and distally, in other PMD patients, resulting in the various sizes of *PLP1* duplications that we observe. The underlying genomic architecture may also be responsible for the grouping of similar duplication size superimposed on the diversity, perhaps reflecting apparent breakpoint-prone genomic regions.

Model for *PLP1* duplication rearrangements

We suggest that LCR–PMDs may be hotspots for stimulating rearrangements, possibly by acting together in the same rearrangement event, and thus render the DNA surrounding the *PLP1* gene unstable and susceptible to rearrangements causing PMD. Interestingly, although most *PLP1* duplications have been reported to be oriented head-to-tail in tandem, we report three potentially complex rearrangements and one interrupted duplication which appears to be inserted near the original reference sequence. Similarly, *PLP1* duplications have been reported to act sometimes as transposons (30,36). We propose a general model (Fig. 10), which incorporates the following: the role of LCR–PMDs in rendering the DNA susceptible to double-strand breaks (DSBs), a mechanism of coupled one-sided homologous single-strand invasion and repair by NHEJ. This model can explain duplications and deletions as well as intra- and inter-chromosomal transposition of the duplicated *PLP1* segment and complex rearrangements.

In this model (Fig. 10), the rearrangement originally occurs during gametogenesis in the ancestral male (33). We propose this event occurs by the induction of a single DSB stimulated by a nearby LCR–PMD. Much like long tract gene conversion (LTGC) (41), and as recently discussed by Woodward *et al.* (19) in the context of *PLP1* duplications, a one-sided single-strand invasion by the broken chromatid occurs in which the sister chromatid is copied. Consistent with what has been found for other *PLP1* duplications (19) and deletions (18), this event is completed by a NHEJ repair mechanism (42).

However, for the cases in which the duplicated segment becomes transposed and inserted either intra-chromosomally, such as the case of interrupted direct duplication inserted close by which we report herein, or inter-chromosomally to autosomes or the Y chromosome, we propose that a second DSB may be stimulated by another nearby LCR–PMD in *trans*, followed by transposition of the duplicated segment to a secondary chromosomal location and repair by NHEJ. Furthermore, our model may also help to account for some complex *PLP1* duplication rearrangements (19), for which more than one proximal or distal breakpoint is predicted. These rearrangements may be explained by part(s) of the duplicated segment being deleted and/or inserted, in a direct or inverted orientation, at either the primary rearrangement site or elsewhere in the genome. For such rearrangements, we hypothesize that at least two LCR–PMDs stimulate at least two DSBs, or potentially greater than two in more complex rearrangements, breaking the duplicated segment into fragments that may become either lost or integrated by NHEJ either intra- or inter-chromosomally, conceivably in inverted or direct orientations and not necessarily in tandem.

CONCLUSIONS

We illustrate that the genomic architecture of the region surrounding *PLP1* is complex, as it contains numerous LCR–PMDs, especially proximal to *PLP1* (Fig. 1). Our data suggest that genomic architectural features, namely LCRs, may stimulate although not necessarily mediate the genomic rearrangements responsible for the majority of PMD cases, as LCRs were identified near the breakpoint regions in a majority of our patients. Specifically, genomic architecture may play an important role in rendering DNA in the *PLP1* region more susceptible to rearrangement, resulting not only in duplications of varying size, but also in the grouping of some duplications of apparently similar size. Duplication rearrangements may be quite common in the human genome; however, only when they result in ascertainable

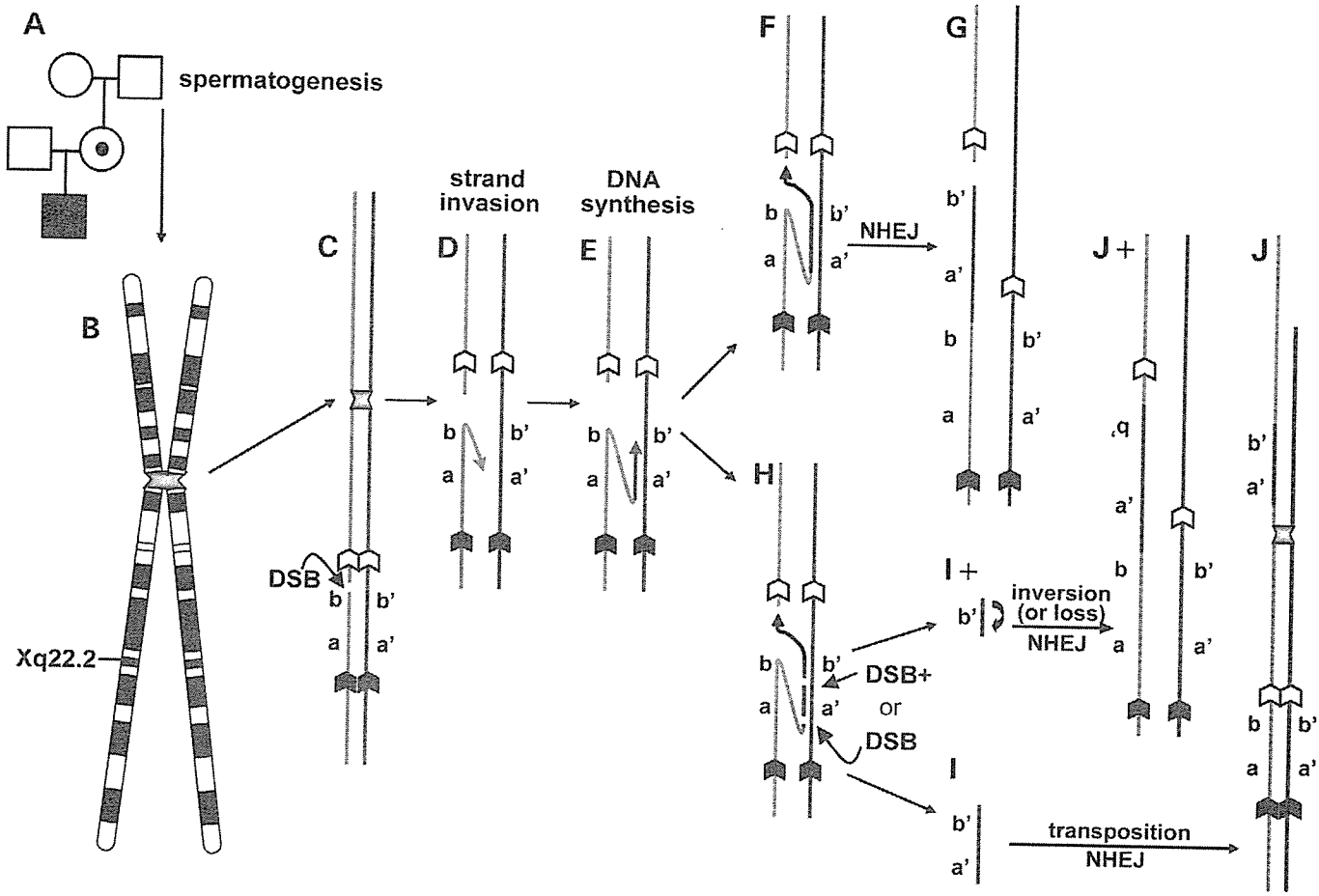

Figure 10. General model for *PLP1* duplication rearrangements. (**A**) The rearrangement originally occurs during spermatogenesis in the ancestral male on his X chromosome, shown as an ideogram in (**B**). (**C**) A DSB is induced near an LCR–PMD (open block arrow). This is followed by (**D**), a strand invasion by the blue chromatid, and (**E**), DNA synthesis off the maroon chromatid template. From here, two pathways can emerge. (Top) (**F**) After DNA synthesis, the chromosome is repaired by NHEJ (**G**). (Bottom) (**H**) A second DSB is induced in *trans* near another LCR–PMD (filled block arrow) at the proximal end of the duplication rearrangement, followed by (**I**), transposition of the duplicated segment and (**J**), repair by NHEJ. (**I+**), Alternatively, DSBs can be induced in *trans* in the middle of the duplication rearrangement, breaking it into segments, which could become inverted (curved arrow) before becoming integrated into the broken chromatid as shown, or which may become lost. (**J+**), repair is completed by NHEJ. Loci are shown as **a** and **b** on the original blue chromatid, and **a′** and **b′** correspondingly on the original maroon chromatid. Segment containing loci **a′** and **b′** on the maroon chromatid is copied, and this copy either is incorporated into the blue chromatid in tandem as shown in (G) (top), or is transposed and incorporated intra-chromosomally, for example, as shown in (J) and (J+) (bottom). Inter-chromosomal transposition is also possible with this model.

human disease phenotypes are they likely to be discovered. *PLP1* duplication rearrangements causing PMD represent one example of many genomic rearrangements causing human disease that are stimulated by complex genomic architecture in the region surrounding the causative dosage-sensitive gene.

MATERIALS AND METHODS

In silico analysis of the *PLP1* region

To define the genomic architecture in the Xq22 region that potentially facilitates the variable *PLP1* duplication events, we performed *in silico* genome sequence analysis covering 8 Mb of repeat-masked DNA sequence from NCBI draft build 35 surrounding the *PLP1* region by BLAST 2 analysis using default parameters (http://www.ncbi.nlm.nih.gov/blast/bl2seq/wblast2.cgi) (43); DNA sequences were obtained from the UCSC Genome Browser (http://genome.ucsc.edu/) (44,45). Specifically, this analysis was performed by dividing the entire analyzed region into ~1 Mb segments; the sequence for each ~1 Mb segment was then compared with itself and with each of the other segments by BLAST 2 to identify LCR sequence and genomic architecture within the analyzed region. We compiled these LCR data from the present analysis together with LCR–PMDA through D (18,19). The sizes of the LCRs detected may be underestimated because each individual identity match does not include interspersed repetitive sequences and low complexity DNA sequences. Additional BLAST 2 analyses of breakpoint clones were performed to further assess for LCRs.

Patients

We obtained samples from 21 PMD patients with *PLP1* duplication and their family members (BAB#) in 17 families

(HOU#) after acquiring informed consent approved by the Institutional Review Board for Human Subject Research at Baylor College of Medicine. Most patients were ascertained because of leukodystrophy and molecular diagnostic evaluation for *PLP1* rearrangement mutations. Clinical details have been published elsewhere for the majority (Table 2). We established lymphoblastoid cell lines from peripheral blood lymphocytes by standard methods for all patients except for patients of BAB2448 and 2390. We performed FISH to confirm *PLP1* duplication status as described (14,46).

Custom array CGH

We prepared and printed DNA from either 38 or 68 BAC and PAC clones tiling an ~5 or ~10 Mb region surrounding *PLP1*, respectively, in addition to control clones from chromosomes 1, 2, 5, 10, 17, X and Y, as described (47). We isolated patient and control genomic DNA either by phenol/chloroform extraction from human cell lines or from peripheral blood using a Puregene kit (Gentra). We digested patient and control genomic DNA with *Dpn*II (New England Biolabs), labeled and hybridized the DNA, and then washed and scanned the slides as described (47). We combined dye reversal pairs for subsequent comparative analysis using a threshold of 0.2 on a log scale.

Pulsed-field gel electrophoresis

We harvested intact lymphoblastoid cells from PMD patient and control individuals and resuspended them in 1% InCert agarose (BMA). We digested DNA in agarose plugs from 5×10^6 cells with *Pme*I or *Nru*I restriction enzymes for 2 days at 37°C (New England Biolabs), followed by separation ranging from 10 kb to 1 Mb on a 1% agarose gel (Bio-Rad) in 0.5X Tris–Borate–EDTA buffer using a Bio-Rad CHEF Mapper. All samples co-migrated with a yeast or lambda chromosome size marker (New England Biolabs). We visualized separated DNA by ethidium bromide (Sigma) staining.

Probe design and preparation

We designed a series of DNA probes to target regions adjacent to the LCRs in the *PLP1* region revealed by *in silico* analysis. Also, we designed additional probes to obtain better coverage. Primer sequences for DNA probes proximal (centromeric) to *PLP1* include: Proximal A, 5′-AGATGTATTCCCTGCCCC ACTAC-3′ and 5′-GTAGCAAGTACAGAGCTTGAGCTAC C-3′; Proximal B, 5′-ACATCCTCACACCACCTGATACTC-3′ and 5′-GAGGCAATGATATCTGTCAGCC-3′; Proximal C, 5′CCCGAAGAATTCCAGCATC-3′ and 5′-CTTTTGCTT C ATCGACAGGG-3′; Proximal D, 5′-GAGTCCTACTCCTG TGCTTGTCTT-3′ and 5′-AGTGTGTGCACATTGTAGGGA G-3′; Proximal E, 5′-GTAAGTTTAGGAAGCAGGGGTCT C-3′ and 5′-GAGGAGGAGACTGCAAGGATAG; Proximal F, 5′-CCTAGCATCGATCTGAACCTATCC-3′ and 5′-GCT GTCACATAACGGGAGTCTAC-3′; and Proximal G, 5′-CC CAGTCTATGAACCTATGGACAG-3′ and 5′-AGGAGTCA GGTCTGTGAGAGATG-3′. Primer sequences for DNA probes distal (telomeric) to *PLP1* include: Distal A, 5′-GAA TGTTGTCAGGTGACCTAGGATT-3′ and 5′-GCAGAGAT GAATTAGGCATGA-3′; Distal B, 5′-ACTGGTAAGGGCT ACTCAACTCAC-3′ and 5′-GAGGTAGTTGGGACTATGT GTGAC-3′; and Distal D, 5′-GTTTGGACCGTGTATTCT CCTC-3′ and 5′-GTCTCTGCTCAAGTTGGGAGTAGT-3′. We amplified these DNA probes by PCR from BAC clone templates prepared by standard alkaline lysis followed by phenol/chloroform extraction, and subsequently isolated the probe DNA by gel extraction (Qiagen).

Southern hybridization

Following the separation of PMD patient and control DNA by PFGE, we transferred DNA to positively charged Sure Blot® Nylon Membranes (Intergen Company) by standard methods for 2 days. We labeled ~200–250 ng of probe DNA with ^{32}P-dCTP (MP Biomedicals) by random priming for at least 2 h at 37°C (Roche). We pre-hybridized membranes with salmon sperm DNA (Sigma) for 4 h and hybridized overnight at 65°C with labeled probes pre-associated with human placental DNA for 1.5–2 h. Subsequently, we analyzed hybridized blots by autoradiography for the presence of bands of expected size and also for bands of varying size, representing recombination-specific junction fragments. We stripped and rehybridized blots with different probes as necessary.

Interphase and metaphase fluorescence *in-situ* hybridization

We harvested cultured lymphoblastoid patient and control cells after Colcemid (Sigma) treatment by standard methods, and dropped them onto glass slides. G-banding was performed by standard methods on all patients with larger duplications except for BAB1327, including BAB2389, 2390, 2396 and 2425. We based our selection of clones to be used as FISH probes for orientation analysis on their presumed full-duplication status determined by custom array CGH described herein. For interphase FISH, we selected BAC clones RP11-1144F22 and RP11-34P3 as FISH probes for duplication orientation analysis of patients BAB1482, 1597, 1334, 1705 and 1707; clones RP11-1123D8 and RP11-462K21 for analysis of patients BAB1261, 1282, 1275 and 1290; clones RP11-1123D8 and RP11-34P3 for analysis of patients BAB1301 and 1305; clones RP11-1123D8 and RP11-454M22 for analysis of patient BAB1420. For metaphase FISH analysis of larger duplications, we selected clones RP11-1001M23 and RP11-462K21 for analysis of patients BAB2389 and 2390; clones CTD-2270O5 and RP11-393D6 for analysis of patient BAB2396; clones RP11-1001M23 and RP11-393D6 for analysis of patient BAB2425. If available, we analyzed the carrier mothers' cells to provide visualization of the signal pattern on the normal X chromosome as a comparison to the duplicated X chromosome.

Each probe pair above has ~51 kb, 323 kb, 314 kb, 694 kb, 3 Mb, 4.5 Mb, and 5 Mb of genomic sequence between them, respectively. We could not test patients BAB1258, 1263 and 1264 for duplication orientation because the furthest duplicated clones, RP11-1123D8 and RP11-34P3, overlap by 84 kb. Orientation analysis was also not done for patient BAB1327. We isolated BAC clone DNA by standard alkaline lysis followed by phenol/chloroform extraction. We labeled

DNA from clones for which pairs have intervening sequence by nick translation either indirectly with digoxigenin (Roche) or biotin (Invitrogen), or directly with SpectrumRed™ or SpectrumGreen™ dUTP (Vysis Inc.). We hybridized probes to interphase and metaphase nuclei on glass slides, counterstained with DAPI (Sigma) in Vectashield (Vector Laboratories Inc.), and visualized the nuclei and metaphase chromosomes by fluorescent microscopy. The order of red and green signals observed, namely red-green-red-green versus red-green-green-red, is indicative of either a direct or inverted duplication, respectively, having occurred in the patient as previously described (48).

Real-time quantitative PCR

As previously described, we performed multiplex real-time quantitative PCR Taqman assays (Applied Biosystems) using a custom probe and primer set designed to ascertain the copy number of a unique region between LCR–PMDA and B (FAM) (29). Assays designed to test the *EIF1AX* gene (FAM) and the RNaseP RNA component *RPPH1* (VIC) were used as X chromosome and loading controls, respectively (Applied Biosystems). Using the following reaction conditions: 95°C for 10 min, followed by 40 cycles of 95°C for 15 s, 60°C for 1 min, we amplified in triplicate 10 ng of genomic DNA. We determined DNA copy number as $2^{-(ddCt)}$ for patients versus a male control.

ACKNOWLEDGEMENTS

We thank the patients and families for their participation in this study, and Sou Saukam for performing G-banding analysis. This work was supported in part by grants from the National Institute of Neurological Disorders and Stroke, NIH (R01 NS27042, J.R.L.), the National Institute for Child Health and Development, NIH (P01 HD38420, J.R.L.), the Baylor College of Medicine Mental Retardation Research Center (HD 2406407), Research Grant for Nervous and Mental Disorders from the Ministry of Health, Labor and Welfare, Japan (16B-1, K.I.), and Health and Labor Science Research Grant, Japan (H18-Kokoro-Ippan-015, K.I.).

Conflict of Interest statement. The authors have no conflicts of interest to declare.

REFERENCES

1. Lupski, J.R. (1998) Genomic disorders: structural features of the genome can lead to DNA rearrangements and human disease traits. *Trends Genet.*, **14**, 417–422.
2. Stankiewicz, P. and Lupski, J.R. (2002) Genome architecture, rearrangements and genomic disorders. *Trends Genet.*, **18**, 74–82.
3. Lupski, J.R. and Stankiewicz, P. (2005) Genomic disorders: molecular mechanisms for rearrangements and conveyed phenotypes. *PLoS Genet.*, **1**, 627–633.
4. Inoue, K., Dewar, K., Katsanis, N., Reiter, L.T., Lander, E.S., Devon, K.L., Wyman, D.W., Lupski, J.R. and Birren, B. (2001) The 1.4-Mb CMT1A duplication/HNPP deletion genomic region reveals unique genome architectural features and provides insights into the recent evolution of new genes. *Genome Res.*, **11**, 1018–1033.
5. Lupski, J.R. (1998) Charcot-Marie-Tooth disease: lessons in genetic mechanisms. *Mol. Med.*, **4**, 3–11.
6. Chen, K.-S., Manian, P., Koeuth, T., Potocki, L., Zhao, Q., Chinault, A.C., Lee, C.C. and Lupski, J.R. (1997) Homologous recombination of a flanking repeat gene cluster is a mechanism for a common contiguous gene deletion syndrome. *Nat. Genet.*, **17**, 154–163.
7. Chen, K.-S., Potocki, L. and Lupski, J.R. (1996) The Smith-Magenis syndrome [del(17)p11.2]: clinical review and molecular advances. *Ment. Retard. Dev. Disabil. Res. Rev.*, **2**, 122–129.
8. Peoples, R., Franke, Y., Wang, Y.-K., Pérez-Jurado, L., Paperna, T., Cisco, M. and Francke, U. (2000) A physical map, including a BAC/PAC clone contig, of the Williams-Beuren syndrome—deletion region at 7q11.23. *Am. J. Hum. Genet.*, **66**, 47–68.
9. Morris, C.A., Demsey, S.A., Leonard, C.O., Dilts, C. and Blackburn, B.L. (1988) Natural history of Williams syndrome: physical characteristics. *J. Pediatr.*, **113**, 318–326.
10. Inoue, K. and Lupski, J.R. (2002) Molecular mechanisms for genomic disorders. *Annu. Rev. Genom. Hum. Genet.*, **3**, 199–242.
11. Garbern, J., Cambi, F., Shy, M. and Kamholz, J. (1999) The molecular pathogenesis of Pelizaeus-Merzbacher disease. *Arch. Neurol.*, **56**, 1210–1214.
12. Hodes, M.E., Pratt, V.M. and Dlouhy, S.R. (1993) Genetics of Pelizaeus-Merzbacher disease. *Dev. Neurosci.*, **15**, 383–394.
13. Inoue, K. (2005) *PLP1*-related inherited dysmyelinating disorders: Pelizaeus-Merzbacher disease and spastic paraplegia type 2. *Neurogenetics*, **6**, 1–16.
14. Inoue, K., Osaka, H., Imaizumi, K., Nezu, A., Takanashi, J.-i., Arii, J., Murayama, K., Ono, J., Kikawa, Y., Mito, T. *et al.* (1999) Proteolipid protein gene duplications causing Pelizaeus-Merzbacher disease: molecular mechanism and phenotypic manifestations. *Ann. Neurol.*, **45**, 624–632.
15. Sistermans, E.A., de Coo, R.F.M., De Wijs, I.J. and Van Oost, B.A. (1998) Duplication of the proteolipid protein gene is the major cause of Pelizaeus-Merzbacher disease. *Neurology*, **50**, 1749–1754.
16. Mattei, M.G., Alliel, P.M., Dautigny, A., Passage, E., Pham-Dinh, D., Mattei, J.F. and Jollès, P. (1986) The gene encoding for the major brain proteolipid (PLP) maps on the q-22 band of the human X chromosome. *Hum. Genet.*, **72**, 352–353.
17. Willard, H.F. and Riordan, J.R. (1985) Assignment of the gene for myelin proteolipid protein to the X chromosome: implications for X-linked myelin disorders. *Science*, **230**, 940–942.
18. Inoue, K., Osaka, H., Thurston, V.C., Clarke, J.T.R., Yoneyama, A., Rosenbarker, L., Bird, T.D., Hodes, M.E., Shaffer, L.G. and Lupski, J.R. (2002) Genomic rearrangements resulting in *PLP1* deletion occur by non-homologous end joining and cause different dysmyelinating phenotypes in males and females. *Am. J. Hum. Genet.*, **71**, 838–853.
19. Woodward, K.J., Cundall, M., Sperle, K., Sistermans, E.A., Ross, M., Howell, G., Gribble, S.M., Burford, D.C., Carter, N.P., Hobson, D.L. *et al.* (2005) Heterogeneous duplications in patients with Pelizaeus-Merzbacher disease suggest a mechanism of coupled homologous and nonhomologous recombination. *Am. J. Hum. Genet.*, **77**, 966–987.
20. Hudson, L.D. (2001) Pelizaeus-Merzbacher disease and the allelic disorder X-linked spastic paraplegia type 2. In Scriver, C.R., Beaudet, A.L., Sly, W.S. and Valle, D. (eds), *The Metabolic and Molecular Basis of Inherited Diseases*, 8th edn. McGraw-Hill, New York, Vol. IV, pp. 5789–5798.
21. Woodward, K., Kendall, E., Vetrie, D. and Malcolm, S. (1998) Pelizaeus-Merzbacher disease: identification of Xq22 proteolipid-protein duplications and characterization of breakpoints by interphase FISH. *Am. J. Hum. Genet.*, **63**, 207–217.
22. Shaw, C.J. and Lupski, J.R. (2004) Implications of human genome architecture for rearrangement-based disorders: the genomic basis of disease. *Hum. Mol. Genet.*, **13**, R57–R64.
23. Stankiewicz, P., Shaw, C.J., Dapper, J.D., Wakui, K., Shaffer, L.G., Withers, M., Elizondo, L., Park, S.-S. and Lupski, J.R. (2003) Genome architecture catalyzes non-recurrent chromosomal rearrangements. *Am. J. Hum. Genet.*, **72**, 1101–1116.
24. Reiter, L.T., Murakami, T., Koeuth, T., Gibbs, R.A. and Lupski, J.R. (1997) The human *COX10* gene is disrupted during homologous recombination between the 24 kb proximal and distal CMT1A-REPs. *Hum. Mol. Genet.*, **6**, 1595–1603.
25. Park, S.-S., Stankiewicz, P., Bi, W., Shaw, C., Lehoczky, J., Dewar, K., Birren, B. and Lupski, J.R. (2002) Structure and evolution of the Smith-Magenis syndrome repeat gene clusters, SMS-REPs. *Genome Res.*, **12**, 729–738.